Title

Prediction of Maternal and Fetal Pharmacokinetics of Dolutegravir and Raltegravir Using Physiologically Based Pharmacokinetic Modeling

Journal

Clinical Pharmacokinetics, 59(11)

ISSN

0312-5963

Authors

Liu, Xiaomei I

Momper, Jeremiah D

Rakhmanina, Natella Y

et al.

Publication Date

2020-11-01

DOI

10.1007/s40262-020-00897-9

Peer reviewed

HHS Public Access

Author manuscript

Clin Pharmacokinet. Author manuscript; available in PMC 2021 November 01.

Published in final edited form as:

Clin Pharmacokinet. 2020 November ; 59(11): 1433–1450. doi:10.1007/s40262-020-00897-9.

Prediction of maternal and fetal pharmacokinetics of dolutegravir and raltegravir using physiologically-based pharmacokinetic modeling

Xiaomei I. Liu[1], **Jeremiah D. Momper**[2], **Natella Y. Rakhmanina**[1,3], **Dionna J. Green**[4], **Gilbert J. Burckart**[5], **Tim R. Cressey**[6,7,8], **Mark Mirochnick**[9], **Brookie M. Best**[2], **John N. van den Anker**[1,10], **André Dallmann**[10,11]

[1]Division of Clinical Pharmacology, Children's National Hospital Washington D.C [2]University of California San Diego Skaggs School of Pharmacy and Pharmaceutical Sciences, La Jolla CA [3]Elizabeth Glaser Pediatric AIDS foundation, Washington, DC [4]Office of Pediatric Therapeutics, US Food and Drug Administration, Silver Spring, MD [5]Office of Clinical Pharmacology, US Food and Drug Administration, Silver Spring, MD [6]PHPT/IRD 174, Faculty of Associated Medical Sciences, Chiang Mai University, Chiang Mai, Thailand [7]Department of Immunology & Infectious Diseases, Boston, Harvard T.H Chan School of Public Health, MA, USA [8]Department of Molecular & Clinical Pharmacology, University of Liverpool, UK [9]Boston University, School of Medicine, Boston, MA [10]Division of Pediatric Pharmacology and Pharmacometrics, University of Basel Children's Hospital, Basel, Switzerland [11]Bayer, Clinical Pharmacometrics, Leverkusen, Germany

Abstract

Background—Predicting drug pharmacokinetics (PK) in pregnant women including placental drug transfer remains challenging. This study aimed to develop and evaluate maternal-fetal physiologically-based PK (PBPK) models for two antiretroviral drugs (ARVs), dolutegravir (DTG) and raltegravir (RAL).

Methods—PBPK models were built with the Open Systems Pharmacology software suite (PK-Sim/MoBi). Different approaches to inform placental drug transfer were applied and compared. Model performance was evaluated using *in vivo* DTG and RAL maternal plasma concentrations during the 2nd and 3rd trimesters and umbilical vein concentrations at delivery. All clinical *in vivo* data were obtained from the International Maternal Pediatric and Adolescent AIDS Clinical Trials (IMPAACT) Network P1026s study.

Corresponding author: Dr. Xiaomei Liu; rph5862@gmail.com.

Disclaimer: The opinions expressed in this article are those of the authors and should not be interpreted as the position of the U.S. Food and Drug Administration or of the National Institutes of Health. No broader FDA policies or perspectives are intended nor should be inferred. The FDA does not recommend any specific PBPK software.

Conflict of Interest/Disclosure: The authors declare no potential conflicts of interest with respect to the research, authorship, and/or publication of this article. Dr. Andre Dallmann is an employee of Bayer AG, a company which is part of the Open Systems Pharmacology (OSP) member team and involved in OSP software development used in this study. The results from this study were presented in part at the American College of Clinical Pharmacology Annual Meeting, Washington DC, September 2018.

Results—The PBPK models successfully predicted plasma concentration-time profiles of DTG and RAL in the 2nd and 3rd trimesters and most predicted PK parameters fell within a 1.33-fold error range. Predicted umbilical vein concentrations of DTG were in reasonable agreement with *in vivo* data but were sensitive to changes in the placental partition coefficient and transplacental clearance.

Conclusion—Maternal-fetal PBPK modeling reliably predicted maternal PK of DTG and RAL during pregnancy. For the fetal PK, data on the unbound fraction of highly protein-bound DTG has proven to be important to adequately capture changes in total clearance *in silico*. More research efforts, along with clinical data, are needed to verify the predictions of fetal PK of ARVs. Overall, the findings suggest that it may be possible to use PBPK models to assess the disposition of ARVs in pregnant women and their fetuses.

Keywords

physiologically-based pharmacokinetics; antiretroviral therapy; UGT1A1; maternal-fetal; pharmacodynamics

1. Introduction

The recommendation to provide all pregnant women living with HIV with antiretroviral therapy (ART) has had a major impact on the prevention of vertical transmission of HIV in the United States (U.S.) and globally. The incidence rate for perinatally acquired HIV infection in the U.S. has decreased from over 5% in 2002 to about 2% in 2013 and to 53 cases in 2015 [1, 2]. The goal of the U.S. Center for Disease Control and Prevention is the complete elimination of perinatal HIV transmission [3]. Perinatal HIV infection still persists globally due to challenges with timely identifying HIV infection and maintaining suppressive ART throughout pregnancy, postpartum and throughout breastfeeding. Providing efficacious ART in to pregnant women is also challenging as physiologic changes during pregnancy can considerably affect the pharmacokinetics (PK) of antiretroviral drugs (ARVs). Indeed, a number of ARVs require a dose adjustment during pregnancy or are not recommended for use in pregnant women because of decreased plasma concentrations or fetal risks [4].

The integrase strand transfer inhibitors (INSTIs) are recommended as first line ART agents in ARV-naïve pregnant women [5]. Their initiation in late pregnancy has also been reported to rapidly achieve viral suppression by the time of delivery [6]. A recent report of the association between dolutegravir (DTG) use at the time of conception with a higher risk of neural tube birth defects in newborns has led to the change in the global and U.S. guideline regarding DTG use in women of child-bearing potential, however still recommending the use of DTG during the 2nd and 3rd trimester of pregnancy [7, 8]. Physiological alterations in pregnancy may lead to reduced maternal plasma concentrations of DTG and RAL which increases the risks of viremia and vertical transmission of HIV.

Understanding the PKs of ARVs in pregnant women facilitates optimal dosing of ART and prevention of viremia and vertical transmission of HIV.

Physiologically-based pharmacokinetic (PBPK) modeling is a promising approach to investigate PK of xenobiotics in special populations where clinical trials are difficult to conduct, such as pregnant women and their fetuses. PBPK models are mechanistic models mapping the model structure to the circulatory system in a biologically plausible manner and integrating extensive information on the anatomy and physiology of the organism as well as physicochemical properties of the xenobiotic. While some pregnancy PBPK models have been previously reported [9], they are still not considered qualified for use in pregnancy because of limited experience. This study aimed to build a maternal-fetal PBPK model for DTG and RAL in order to predict their PK profiles in pregnant women during the 2nd and 3rd trimester, as well as in their fetuses at delivery. This study presents a new process to parameterize unknown parameters describing placental transfer (specifically, the transplacental clearance and drug partitioning between the fetus and the mother in the placenta) by combining recently proposed *in silico* techniques relying exclusively on *in vitro* information; additionally, drug partitioning between the fetus and the mother was estimated according to more conventional approaches and the results obtained from these methods were compared to clinical data. Predicted PK profiles were evaluated through comparison with *in vivo* data obtained from the International Maternal Pediatric and Adolescent AIDS Clinical Trials (IMPAACT) Network P1026s study (trial number: NCT00042289).

2. Materials and Methods

2.1 Software

PBPK models were developed using the open source software tool Open Systems Pharmacology (OSP) version 8.0 (http://www.open-systems-pharmacology.org/) which makes formerly commercial software PK-Sim® and MoBi® available as freeware under the GPLv2 License. All source code and the herein developed models will be made publicly available on GitHub (accessible via www.open-systems-pharmacology.org). WebPlotDigitizer (http://automeris.io/WebPlotDigiti-zer/) was used to extract data from published figures and convert them into digital format. The open source software PaDEL-Descriptor [10] was used to estimate molecular descriptors of DTG and RAL and the free software R (version 3.4.1, R Foundation for Statistical Computing, Vienna, Austria; http://www-.r-project.org) was used for non-compartmental analysis and graphics creation.

2.2 General Workflow

The workflow for the development of the pregnancy PBPK model has been previously described in detail [11] and is schematically shown in Fig S1. Briefly, a PBPK model was initially developed for a virtual non-pregnant population and evaluated by comparing simulation results with the observed *in vivo* PK data in non-pregnant subjects reported in the comparison studies. Thereafter, the non-pregnant PBPK model was translated to pregnancy by substituting the standard model structure with the pregnancy structure and parametrizing the model for the respective gestational age as described before. [11] PK predictions in pregnant women were evaluated by comparison with *in vivo* PK data obtained from clinical trials of IMPAACT P1026s.

2.3 Development of PBPK pregnancy models

2.3.1 Dolutegravir—DTG is dosed at 50 mg once daily as an orally administered tablet in both pregnant and non-pregnant treatment-naïve and treatment-experienced adult patients without INSTIs resistance. DTG is primarily eliminated by metabolism through various enzymes including UGT1A1, UGT1A3, UGT1A9 and CYP3A4 (~ 51%, ~ 2.8%, ~ 5.5% and ~ 21% of the dose, respectively[12]). In the developed model, the contribution of UGT1A3 and 1A9 to total glucuronidation was combined into the biotransformation pathway mediated by UGT1A1. Finally, to obtain dose fractions summing up to 1.0, the dose fraction metabolized via UGT1A1 was increased to 0.79 based on the assumption that the reported value (0.51) may be underestimated due to hydrolyzation and back conversion of the glucuronide to DTG in the feces, as discussed elsewhere[12]. PBPK model input parameters for DTG are listed in Tab. 1.

In the pregnancy PBPK model, physiologic parameters were adjusted to the respective stage of pregnancy as described previously [13]. Additionally, the reference concentrations of UGT1A1 and CYP3A4 (quantifying the concentrations of these enzymes in the model) were increased to reflect induction of these enzymes. Specifically, CYP3A4 reference concentration was increased by a factor of 1.60 in the 2nd and 3rd trimesters and UGT1A1 reference concentration by a factor of 1.75 in the 2nd trimester and 1.92 in the 3rd trimester [14, 15]. The fraction unbound of DTG, averaging 0.0070 in non-pregnant subjects,[16] was also adjusted based on the albumin concentration measured in the herein investigated study subjects. Specifically, the mean albumin concentration measured in the 2nd trimester, 3rd trimester and 6 – 12 weeks postpartum was 34.4 g/L, 32.8 g/L and 41.4 g/L, respectively. Using a previously presented scaling approach [13], these measurements resulted in a fraction unbound of 0.0084 and 0.0088 in the 2nd and 3rd trimester, respectively. Additional information on model development and translation to pregnancy can be found in the Supplemental Material.

PK simulations in the non-pregnant population were evaluated by comparison with *in vivo* data obtained from eight clinical studies reported in the literature that investigated the PK of DTG in a total of 22 different groups of non-pregnant subjects after single and multiple oral administrations of 2 to 100 mg as granule suspension or 50 mg as tablet in fasted or fed state [17-26].

In pregnant women, the PK was predicted in 2 different gestational age groups of non-laboring pregnant women in the 2nd trimester (median gestational age [range]: 23.5 [20 - 25] weeks) and 3rd trimester (median gestational age [range]: 33 [30-37] weeks), and in women in labor (median gestational age [range]: 38 [35 - 42] weeks). Drug concentrations in the blood plasma of the umbilical vein were predicted in the laboring pregnant women group.

2.3.2 Raltegravir—RAL is dosed at 400 mg twice daily or 1200 mg once daily as an orally administered tablets in both pregnant and non-pregnant treatment-naive and treatment-experienced adult patients. RAL is primarily eliminated by metabolism catalyzed by UGT1A1 and UGT1A9 (~70% and 11% of the administered dose, respectively[27]). Additionally, approximately 9% is eliminated unchanged through the kidneys [27]. The input parameters and their values for the RAL PBPK model are listed in Tab. 1. Additional

information can be found in the Supplemental Material. The non-pregnant PBPK model for RAL was obtained from the OSP GitHub repository (https://github.com/Open-Systems-Pharmacology/Raltegravir-Model/releases) where an extensive description and evaluation of the model can be found.

In the pregnancy PBPK model, physiologic parameters and the reference concentrations of UGT1A1 were adjusted to the respective stage of pregnancy as described above. Since no information on the effect of pregnancy on UGT1A9 could be found, this enzyme was not induced in the presented model. Similar to DTG, the fraction unbound of RAL, averaging 0.17 in non-pregnant adults,[28] was adjusted based on the mean albumin concentration measured in the 2nd trimester, 3rd trimester and 6 – 12 weeks postpartum (34.1 g/L, 32.4 g/L and 41.4 g/L, respectively) resulting in a fraction unbound of 0.198 and 0.206 in the 2nd and 3rd trimester, respectively. Additional information on model development and translation to pregnancy can be found in the Supplemental Material.

In pregnant women, the PK were predicted in 2 different gestational age groups of non-laboring pregnant women in the 2nd trimester (median gestational age [range]: 23.5 [21 - 26] weeks) and the 3rd trimester (median gestational age [range]: 34 [30 - 38] weeks), and in women in labor (median gestational age [range]: 38 [36 - 40] weeks). Drug concentrations in the blood plasma of the umbilical vein were predicted in the laboring pregnant women group.

2.3.3 Clinical in vivo data in pregnant women living with HIV—

The clinical *in vivo* data were from the IMPAACT network P1026s study. Intensive steady state blood samples for PK assessment were collected in the 2nd trimester (optional), 3rd trimester, and postpartum, and single maternal and cord blood samples were collected at delivery. Further information can be found in Tab. S1 in the supplement. The performance of the PBPK model to predict drug concentrations in the umbilical cord was evaluated via comparison with clinical *in vivo* data collected at delivery. The protocol for this study was approved by the responsible Institutional Review Boards. The IMPAACT P1026s study is an ongoing (trial number: NCT00042289), multicenter, phase IV prospective study and a part of the herein reported data has been previously published [29, 30]. In addition, clinical PK data in pregnant women reported by Waitt et al [31] and Blonk et al.[32] were used to evaluate the steady-state PK predictions of DTG around gestational week 31 and of RAL around gestational week 33, respectively.

2.4 Parameterization of placental transfer

Placental transfer kinetics of DTG and RAL was mathematically described as reported previously [33] (also described in detail in the supplement) and informed by *in silico* methods. Specifically, the transplacental clearance (D_{pl}) was estimated from the approach suggested by Zhang et al. [34] which estimates the transplacental clearance from the permeability measured in Caco2 cell lines. For DTG, Caco2 cell permeability (2.5 E-6 cm/s) was obtained from Grießinger et al. [35] resulting in a transplacental clearance of 0.43 L/min. For RAL, a Caco2 cell permeability of 7.3E-6 cm/s was reported [36] resulting in a transplacental clearance of 1.24 L/min.

Four different methods were used to estimate the partition coefficient between the fetal intracellular space and the maternal blood plasma of the placenta in the model ($K_{fc:mp}$), in particular: i) the "PK-Sim Standard" calculation method;[37] ii) the method proposed by Poulin & Theil;[38, 39] iii) the method proposed by Rodgers & Rowland;[40, 41] and vi) a quantitative structure-activity relationship (QSAR) model for the fetal-maternal blood concentration ratio which was used as surrogate for $K_{fc:mp}$. The fetal-maternal blood concentration ratio was calculated according to the QSAR model suggested by Takaku et al. [42] which uses molecular weight, polar surface area, and maximum E-state of hydrogen atom in the compound (H_{max}) to estimate the fetal: maternal blood concentration ratio. Using the open source software PaDEL-Descriptor [10], the polar surface area was estimated to be 95.9 $Å^2$ and 147 $Å^2$ for DTG and RAL, respectively; and H_{max} 0.93 and 0.82 for DTG and RAL, respectively. Physiological values required for calculating the partition coefficients, e.g. tissue composition, are published elsewhere[13]. The values for $K_{fc:mp}$ calculated according to each of the four methods are listed in Tab. 2.

2.5 Parameterization of placental metabolism

In the model, the amount of CYP3A4, UGT1A1 and UGT1A9 in the fetal part of the placenta and the fetal body was informed based on reported data from previous studies that quantified the mRNA level of CYP3A4 [43] as well as protein levels and the activity of UGT1A1 [44, 45] in various human tissues, including the adult liver, placenta and fetal liver. Further information can be found in the supplement. The protein amounts listed in Tab. 3 were then incorporated in the pregnancy PBPK model. As discussed further below, the difference of fraction unbound between fetus and mother was not considered because of the high uncertainty in fetal protein binding.

2.6 Evaluation of PBPK models

The PBPK models were evaluated through visual comparison of observed *in vivo* plasma concentration-time profiles with the concentrations simulated in non-pregnant subjects or in pregnant women. Additional visual assessments included goodness-of-fit (GOF) and residuals vs time plots. Ratios of simulated to observed PK parameters were estimated and the number of ratios falling within a 1.33-fold error range (i.e. $0.75 \leq \text{ratio} \leq 1.33$) was given. An extensive evaluation of the non-pregnant PBPK model for RAL has been previously published on GitHub (https://github.com/Open-Systems-Pharmacology/Raltegravir-Model).

2.7 Sensitivity analysis

Local sensitivity analyses were conducted to assess how the uncertainty in specific parameters might propagate to the final model output (plasma concentration-time profiles in the 2nd and 3rd trimester of pregnancy or at delivery). The following parameters were included in local (univariate) sensitivity analyses: UGT1A1 induction, the transplacental clearance, and the gastric emptying time of the mother at delivery.

3. Results

3.1 Non-pregnant PBPK models

3.1.1 Dolutegravir: The simulated plasma concentration-time profiles of DTG in non-pregnant populations following administration of 50 mg tablet QD in fed state (i.e. the same dosing regimen than in pregnant women) are shown in Fig. 1, while Fig. S2 shows simulated plasma concentration-time profiles following other dosing regimens. The ratios of simulated to observed PK parameters in non-pregnant subjects are listed in Tab. 4 together with the absolute simulated and observed values. All simulated AUC values fell within a 1.33-fold error range. Eleven out of 13 (85%) C_{max} values fell within a 1.33-fold error range. Time to C_{max} (t_{max}) was somewhat less accurately simulated, but still 10 out of 13 (77%) simulated values fell within a 1.33-fold error range. This model was subsequently translated to pregnant women.

3.1.2 Raltegravir: An extensive evaluation of the non-pregnant PBPK model for RAL can be found in the model repository on GitHub (https://github.com/Open-Systems-Pharmacology/Raltegravir-Model); here, only a limited number of results is shown. The simulated plasma concentration-time profiles of RAL in non-pregnant populations following administration of 400 mg tablet BID in fed state (i.e. the same dosing regimen as in pregnant women) are shown in Fig. 2. In addition, Fig. S3 shows simulated plasma concentration-time profiles following other dosing regimens. The ratios of simulated to observed PK parameters in non-pregnant subjects are listed in Tab. 4 together with the absolute simulated and observed values. Five out of ten (50%) simulated AUC value fell within a 1.33-fold error range (i.e. $0.75 \leq \text{ratio} \leq 1.33$). For C_{max} and t_{max}, 3 out of 10 (30%) simulated values were within this range. While there were some difficulties to describe the data of few clinical studies, the model was overall deemed adequately to describe RAL PK when also considering additional studies with different posology (see Fig. S3 and additional information available on https://github.com/Open-Systems-Pharmacology/Raltegravir-Model). Hence, this model was subsequently translated to pregnant women.

3.2 Pregnancy PBPK models in the 2nd and 3rd trimester

3.2.1 Dolutegravir: The predicted DTG plasma concentration-time profiles in the 2nd and 3rd trimesters of pregnancy are shown in Fig. 3 and in Fig. S5 with clinical data reported by other research groups. Fig. 4 shows the GOF plot for the model-predicted DTG plasma concentrations in non-pregnant and pregnant women. All but 2 out of 16 (87.5%) geometric mean DTG concentrations were predicted within a two-fold error range. The absolute values as well as ratios of predicted to observed $AUC_{0\text{-}24}$, C_{max} and t_{max} in the pregnant populations are listed in Tab. 4. The $AUC_{0\text{-}24}$ of 2nd trimester and C_{max} of 2nd trimester and 3rd trimester were predicted within a 1.33-fold error range. The $AUC_{0\text{-}24}$ in 3rd trimester was predicted within a 1.5-fold error range; similar to simulations in non-pregnant subjects, t_{max} was less accurately predicted in the 2nd trimester, but again in the 1.33-fold error range in the 3rd trimester. Tab. S2 provides an overview of additional PK parameters simulated in non-pregnant and pregnant populations. Variability was reasonably described by the model; specifically, the predicted 5th – 95th percentile range contained 76% of all observed

concentration values in the 2nd trimester and 69% of all observed concentration values in the 3rd trimester.

3.2.2 Raltegravir: The predicted RAL plasma concentration-time profiles in the 2nd and 3rd trimesters of pregnancy are shown in Fig. 5 and in Fig. S5 with clinical data reported by other research groups. Fig. 6 shows the GOF plot for the model-predicted RAL plasma concentrations in non-pregnant and pregnant women with the residuals versus time. All but 1 of out 14 (92.9%) geometric mean RAL concentrations in pregnant populations were predicted within a 2-fold error range. The observed and predicted values for $AUC_{0\text{-}24}$, C_{max} and t_{max} as well as their ratios are listed in Tab. 4. These geometric mean PK parameters were all predicted within a 1.33-fold error range in the 2nd and 3rd trimester. Tab. S2 provides an overview of additional PK parameters simulated in non-pregnant and pregnant populations. Variability was underestimated by the model; specifically, the predicted 5th – 95th percentile range contained only 64% of all observed concentration values in the 2nd trimester and 55% of all observed concentration values in the 3rd trimester.

3.3 Pregnancy PBPK models for delivery

3.3.1 Dolutegravir—Maternal and umbilical cord plasma concentrations of DTG predicted at delivery are shown in Fig 3C & 3D, respectively. Fourteen out of 20 maternal samples at delivery fell within the 2-fold error range of the predicted mean concentration, and 8/20 maternal samples fell within the 1.5-fold error range. Seventeen out of 20 cord samples fell within the 2-fold error range of the predicted mean concentration and 11/20 cord samples fell within the 1.5-fold error range.

The predicted steady-state exposure was higher in the fetus compared to the mother; specifically, the predicted geometric AUC_{tau} was 40.99 mg h/L in the umbilical vein and 26.84 mg h/L in the maternal plasma.

3.3.2 Raltegravir—Maternal and umbilical cord plasma concentrations of DTG predicted at delivery are shown in Fig 5C & 5D, respectively. Five out of 24 maternal samples fell within the 2-fold error range of the predicted mean and 7/23 fetal samples fell within the 2-fold error (one fetal sample was missing). The predicted steady-state exposure was higher in the fetus compared to the mother; specifically, the predicted geometric AUC_{tau} was 4.73 mg h/L in the fetus and 3.16 mg h/L in the maternal plasma.

3.4 Sensitivity analyses

Local sensitivity analyses are shown in Figs S4, S6 and S7. The sensitivity analysis of UGT1A1 induction of DTG and RAL shown in Fig. S4 indicated that, within the tested range, UGT1A1 induction had a moderate influence on the predicted PK of DTG and RAL during pregnancy. The sensitivity analysis for the placenta diffusion clearance of DTG shown in Fig. S6 suggests that it was a sensitive model parameter for DTG but not for RAL. Although no sensitivity analysis was conducted for $K_{fc:mp}$, Fig. 3D and 5D show the predicted PK in the umbilical vein when different values for $K_{fc:mp}$ are incorporated in the model. Further sensitivity analysis on the gastric emptying time of the mother are shown in

Fig S7 indicating that a prolonged gastric emptying time increases both maternal and fetal exposure.

4. Discussion

In this study, maternal-fetal PBPK models were developed for DTG and RAL and evaluated by comparing predicted concentrations to those observed in the maternal plasma during the 2nd and 3rd trimester and in the maternal and umbilical cord plasma at delivery. Development of these models followed a standard workflow comprising the initial establishment of a non-pregnant PBPK model and the subsequent translation to pregnancy.

The PK of DTG predicted in pregnant, non-laboring women was in good agreement with clinical data obtained at different stages of pregnancy (Fig. 3 and Tab. 4). While most PK parameters were adequately predicted, t_{max} in the 2nd trimester was somewhat overestimated and AUC_{tau} underestimated in the 3rd trimester (Tab. 4, Fig. 3). The reason for the decrease in t_{max} in the 2nd (but not the 3rd) trimester *in vivo* is yet unknown and further clinical studies strictly controlling for food intake could help to elucidate that point. The underestimation of AUC_{tau} in the 3rd trimester could mainly be ascribed to an overestimation of total body clearance. Combined with the results from the sensitivity analysis on UGT1A1 induction (Fig. S4), this finding emphasizes that UGT1A1 induction may be lower than expected here and that changes in the fraction unbound are, at least for DTG, the main driver of increased total clearance which is consistent with recent findings in the literature [46]. The PK of RAL was generally well predicted in pregnant, non-laboring women (Fig. 5) and all mean PK parameters were predicted within a 1.33-fold error range (Tab. 4). However, variability was underestimated, especially in the first hours after drug administration indicating that the model did not fully capture variability related to drug absorption.

UGT1A1 plays an important role in the metabolism of both DTG and RAL. While *in vitro* experiments support an increase in UGT1A1 expression mediated by rising progesterone levels during pregnancy [47], there is scarce information on quantitative changes in UGT1A1 expression during pregnancy *in vivo*. In a previous pregnancy PBPK model for acetaminophen (paracetamol), UGT1A1 was assumed to be induced by a factor of 1.75 in the 2nd trimester and 1.92 in the 3rd trimester [15] and these induction factors were incorporated here. Due to the relatively high uncertainty in these factors, a local sensitivity analysis was conducted (Fig. S4). While maternal PK of DTG was moderately sensitive to alterations in UGT1A1 expression, maternal PK of RAL was rather weakly affected by these alterations. Additional studies dedicatedly investigating UGT1A1 activity changes in pregnant women are needed to better define whether and to which extent UGT1A1 is induced during pregnancy. Clinical studies on different UGT1A1-metabolized drugs, e.g. carvedilol and irinotecan, could be helpful to answer this question.

A key objective of this study was to predict fetal PK of DTG and RAL in the maternal plasma and venous blood plasma of the umbilical cord at delivery. To this end, different approaches to inform placental transfer kinetics were tested. Specifically, D_{pl} (the placental diffusion clearance) was estimated from Caco-2 permeability [34] and $K_{fc:mp}$ (the fetal intracellular-to-maternal plasma partition coefficient in the placenta) was calculated either

by previously reported methods for estimation of organ-to-plasma partition coefficients [37]' [38, 39]'[40, 41] or by a previously reported QSAR approach [42] assuming that the fetal-maternal blood concentration ratio can be used as surrogate for $K_{fc:mp}$. Hence, placental transfer was exclusively informed by *in vitro* and *in silico* methods. This has the strength to bypass the need for additional *ex vivo* experiments, such as the placental cotyledon perfusion experiment, but it also displays several shortcomings. For example, DTG is a substrate of P-glycoprotein (P-gp; multidrug resistance protein 1 [MDR1]), one of the major efflux transporters expressed in the placenta[48], and the effect of this transporter may not be consistently accounted for by the proposed approach for estimation of D_{pl}. Although drug transporters are present in Caco-2 cell lines, their expression may differ from that in placental cells and may not correlate with the placental protein amount *in vivo* [48], thereby distorting the estimated value for D_{pl}. Indeed, the limited data available seem to indicate that the expression of P-gp normalized to that of the housekeeping gene GAPDH (glyceraldehyde-3-phosphate dehydrogenase) is slightly higher in Caco-2 cells [49-52] than in the human term placenta [53, 54]. The higher P-gp expression in Caco-2 cells may consequently have contributed to an underestimation of D_{pl}. As shown in Fig. S6, D_{pl} was a sensitive model parameter for DTG but not for RAL. Unfortunately, the low number of observed data and the high variability therein, especially in the terminal phase, preclude any sound conclusion on whether the estimated D_{pl} for DTG should be higher. This illustrates the importance of developing new modeling approaches that delineate passive diffusion and active transport across the placenta.

The presented findings in Fig. 3D and 5D show that the various methods to estimate $K_{fc:mp}$ yield largely different predictions of umbilical vein concentrations. Given the relatively small size of the fetus, maternal plasma concentrations were barely affected by different $K_{fc:mp}$ values (Fig. 3C and 5C). In general, the small amount of clinical data hindered a thorough evaluation of these predictions and more data are clearly needed, ideally from different tissues (e.g. the maternal plasma, placenta and umbilical vein) to better asses the predictive performance of these models. Nonetheless, keeping this limitation in mind, those models that informed $K_{fc:mp}$ via the Poulin & Theil method or the QSAR approach appeared to predict umbilical vein concentration better than the other models. Umbilical concentrations of DTG appeared to be adequately predicted by these models (Fig 3D), but RAL concentrations were generally underestimated, predominantly because maternal concentrations were also underestimated (Fig 5C and D). This finding stresses the importance of the maternal PK on fetal drug exposure indicating that the main elimination pathway of the fetus is transfer over the placenta back in the mother.

RAL concentrations in the maternal plasma and umbilical vein were especially underestimated after 12 h (i.e. the dosing interval). One reason for the underestimation of maternal RAL plasma concentrations at delivery appeared to be the relatively fast absorption in the model. While the PBPK models for non-laboring women incorporated a fed state to reflect the fact that no restrictions on food intake were imposed in the clinical study, the PBPK model for laboring women incorporated the fasted state (assuming that food intake prior to the onset of labor and delivery is implausible). However, gastric passage of RAL (as well as DTG) was nonetheless delayed in the PBPK model at delivery because there is some evidence that gastric emptying and drug absorption from the gastrointestinal tract are slowed

during labor [55]'[56, 57]. Specifically, Whitehead et al. reported a 3-fold delay in acetaminophen t_{max} in pregnant women (n=36) during labor when compared with 2 h post-delivery women (n=17) [57]. Based on this observation, a 3-fold delay in gastric emptying time was incorporated in the presented PBPK models for RAL and DTG which may not have been enough to reflect the delay in drug absorption. Unfortunately, little clinical data is available for the first few hours after drug administration which complicates a proper assessment of alterations in drug absorption during delivery. As discussed elsewhere in greater detail [9, 58], the effect of pregnancy on drug absorption is poorly understood. The potential effect of delivery – on top of that during pregnancy – further complicates the situation. Once informative clinical data are available, PBPK models applied to the peripartum period could investigate such effects and refine the understanding of physiological changes affecting drug absorption as well as other PK processes.

Ex vivo cotyledon perfusion experiments constitute another important source of information for parameterization of placental transfer in PBPK models [59-61]. One of the advantages is possible to estimate the fraction unbound of the compound in placenta. Yet, data from these experiments are not always available for the studied drug and in other cases they may not translate into meaningful PBPK predictions. For example, although DTG was used in a previous *ex vivo* cotyledon perfusion experiment, the transfer was observed to be very slow and apparent equilibrium concentrations were not reached after 3 hours [62]. These authors discussed that one reason for the slow transfer could have been equal albumin concentrations in the maternal and fetal compartments. Indeed, differences in maternal and fetal protein binding can be critical determinants for placental transfer and equilibrium concentrations reached in steady state [63].

Since only the free drug fraction crosses the placenta, it can be expected that, for highly protein-bound drugs, an increase in the fetal fraction unbound is associated with a decrease in total concentrations at steady-state because the bound drug concentration diminishes. Therefore, maternal-fetal PBPK should ideally consider such differences between the drug's fraction unbound in the maternal and fetal plasma. However, although technically possible in the herein used model, little is known about changes in the fetal fraction unbound. While umbilical cord concentrations of fetal albumin and α-fetoprotein (AFP) can in principle be easily measured from plasma samples obtained at delivery, it is unclear whether fetal albumin and α-fetoprotein display the same affinity to drugs than adult albumin. There is evidence that, compared to adult albumin, fetal albumin has a different binding affinity to several drugs [64, 65] and that AFP lacks specific drug-binding sites [66, 67]. This complicates an estimation of a drug's unbound fraction in the fetal plasma. To correctly parameterize placental transfer of highly protein-bound drugs in PBPK models, clinical data of the fetal fraction unbound *in vivo* are clearly needed. These data could then either be directly applied to inform specific PBPK models or to develop and train novel *in silico* approaches for prediction of the fetal fraction unbound.

On May 18th, 2018, the US FDA released a warning letter [68] that DTG may cause serious neural tube birth defects involving the brain, spine, and spinal cord. The preliminary observations were found in a study in Botswana in women who received DTG at the time of conception [68, 69]. Although the mechanism leading to teratogenicity of DTG is not yet

understood, one hypothesis is that DTG affects folic acid binding to the folate receptor α, thereby reducing folic acid concentrations in the fetus [70]. Since folic acid is essential for neural tube development, a reduction in folic acid can potentially cause neural tube defects in the fetus. According to *in vitro* results presented by Zamek et al. [70], free DTG concentrations of approximately 37 μM are associated with a 36% inhibition of folate receptor α. To set these figures in the *in vivo* context, the presented PBPK model was extrapolated to the 6th gestational week while assuming an induction of UGT1A1 by 33% in the first trimester, as suggested previously [15]. Unbound DTG concentrations were then predicted in the maternal blood of the placenta. The maximum unbound DTG concentration predicted in steady state was 0.06 μM at the 6th gestational week. Using a simple Emax-model fitted to the data reported by Zamek et al. [70] (fitted values are Emax: 1.0; EC50: 1276 μM) , this DTG concentration translates into an inhibition of the folate receptor α by approximately 7 %. It should be noted, though, that this value is based on predicted concentrations that cannot be evaluated because of lacking clinical data and it should therefore not be used to guide dosing decisions. Yet, this example illustrates how PBPK modeling can theoretically contribute to support decision making for the use of DTG during pregnancy. However, this example also emphasizes the need for clinical data to support the confidence of model-based predictions.

5. Conclusion

The developed PBPK models successfully predicted the mean PK profile at different stages of pregnancy by integrating prior knowledge of the pregnancy-related effects on relevant physiological parameters and apparent enzyme activity. Importantly, umbilical vein concentrations were predicted by integrating information solely from *in vitro* or *in silico* techniques. This is the first study evaluating the applicability of standard equations for predicting the fetal-maternal partition coefficient in the placenta. The presented models provide new mechanistic insights in the PK of RAL and DTG during pregnancy which can be conceptually generalized and applied to other drugs. The findings also stress the importance of measuring the unbound fraction for highly protein-bound drugs in both the maternal and fetal plasma when clinical trials are conducted in pregnant populations to facilitate the proper parameterization of PBPK models. Ultimately, verified PBPK models may be used to support informed decision making when clinical trials are designed in this frequently ignored population or when sound and consistent information from trials is lacking.

Supplementary Material

Refer to Web version on PubMed Central for supplementary material.

Acknowledgements:

The authors would like to thank Dr. Ibrahim Ince (Bayer AG) for providing the non-pregnant PBPK model for raltegravir via upload on OSP GitHub.

Funding: Overall support for the International Maternal Pediatric Adolescent AIDS Clinical Trials Network (IMPAACT) was provided by the National Institute of Allergy and Infectious Diseases (NIAID) with co-funding from the *Eunice Kennedy Shriver* National Institute of Child Health and Human Development (NICHD) and the

National Institute of Mental Health (NIMH), all components of the National Institutes of Health (NIH), under Award Numbers UM1AI068632 (IMPAACT LOC), UM1AI068616 (IMPAACT SDMC) and UM1AI106716 (IMPAACT LC), and by NICHD contract number HHSN275201800001I. The NIH awards numbers 5T32HD087969-03 and 5T32HD087969-02 also support this project.

References

1. Taylor AW, Nesheim SR, Zhang X, Song R, Fitzharris LF, Lampe MA , et al. Estimated Perinatal HIV Infection Among Infants Born in the United States, 2002-2013. JAMA Pediatr. 2017; 171(5): 435–442. [PubMed: 28319246]
2. Nesheim SR, Fitzharris LF, Lampe MA, Gray KM. Reconsidering the Number of Women With HIV Infection Who Give Birth Annually in the United States. Public Health Rep. 2018; 133(6): 637–643. [PubMed: 30265616]
3. Nesheim S, Taylor A, Lampe MA, Kilmarx PH, Fitz Harris L, Whitmore S , et al. A framework for elimination of perinatal transmission of HIV in the United States. Pediatrics. 2012; 130(4): 738–44. [PubMed: 22945404]
4. Caritis SN, Bastian JR, Zhang H, Kalluri H, English D, England M , et al. An evidence-based recommendation to increase the dosing frequency of buprenorphine during pregnancy. Am J Obstet Gynecol. 2017; 217(4): 459 e1–459 e6. [PubMed: 28669739]
5. Krishna R, East L, Larson P, Valiathan C, Deschamps K, Luk JA , et al. Atazanavir increases the plasma concentrations of 1200 mg raltegravir dose. Biopharm Drug Dispos. 2016; 37(9): 533–541. [PubMed: 27696440]
6. Rahangdale L, Cates J, Potter J, Badell ML, Seidman D, Miller ES , et al. Integrase inhibitors in late pregnancy and rapid HIV viral load reduction. Am J Obstet Gynecol. 2016; 214(3): 385 e1–7. [PubMed: 26928154]
7. World Health Organization: Update of recommendations on first- and second-line antiretroviral regimens. Access at https://www.who.int/hiv/pub/arv/arv-update-2019-policy/en/ (accessed on November 18, 2019). 2019;
8. National Institutes of Health: Recommendations for the Use of Antiretroviral Drugs in Pregnant Women with HIV Infection and Interventions to Reduce Perinatal HIV Transmission in the United States. Access at: https://aidsinfo.nih.gov/guidelines/html/3/perinatal/0 (accessed on November 18, 2019). 2018;
9. Dallmann A, Pfister M, Van Den Anker J, Eissing T. Physiologically Based Pharmacokinetic Modeling in Pregnancy: A Systematic Review of Published Models. Clin Pharmacol Ther. 2018; 104(6): 1110–1124. [PubMed: 29633257]
10. Yap CW. PaDEL-descriptor: An open source software to calculate molecular descriptors and fingerprints. Journal of computational chemistry. 2011; 32(7): 1466–1474. [PubMed: 21425294]
11. Dallmann A, Solodenko J, Ince I, Eissing T. Applied Concepts in PBPK Modeling: How to Extend an Open Systems Pharmacology Model to the Special Population of Pregnant Women. CPT Pharmacometrics Syst Pharmacol. 2018; 7(7): 419–431. [PubMed: 29569837]
12. Reese MJ, Savina PM, Generaux GT, Tracey H, Humphreys JE, Kanaoka E , et al. In vitro investigations into the roles of drug transporters and metabolizing enzymes in the disposition and drug interactions of dolutegravir, a HIV integrase inhibitor. Drug Metab Dispos. 2013; 41(2): 353–61. [PubMed: 23132334]
13. Dallmann A, Ince I, Meyer M, Willmann S, Eissing T, Hempel G. Gestation-Specific Changes in the Anatomy and Physiology of Healthy Pregnant Women: An Extended Repository of Model Parameters for Physiologically Based Pharmacokinetic Modeling in Pregnancy. Clin Pharmacokinet. 2017; 56(11): 1303–1330. [PubMed: 28401479]
14. Dallmann A, Ince I, Coboeken K, Eissing T, Hempel G. A Physiologically Based Pharmacokinetic Model for Pregnant Women to Predict the Pharmacokinetics of Drugs Metabolized Via Several Enzymatic Pathways. Clin Pharmacokinet. 2018; 57(6): 749–768. [PubMed: 28924743]
15. Mian P, Van Den Anker JN, Van Calsteren K, Annaert P, Tibboel D, Pfister M , et al. Physiologically Based Pharmacokinetic Modeling to Characterize Acetaminophen Pharmacokinetics and N-Acetyl-p-Benzoquinone Imine (NAPQI) Formation in Non-Pregnant and Pregnant Women. Clin Pharmacokinet. 2019; doi: 10.1007/s40262-019-00799-5.

16. Center For Drug Evaluation And Research: Clinical Pharmacology and Biopharmaceutics Review (s). Access at: https://www.accessdata.fda.gov/drugsatfda_docs/nda/2013/204790Orig1s000ClinPharmR.pdf (accessed on October 8, 2019).
17. Castellino S, Moss L, Wagner D, Borland J, Song I, Chen S , et al. Metabolism, excretion, and mass balance of the HIV-1 integrase inhibitor dolutegravir in humans. Antimicrob Agents Chemother. 2013; 57(8): 3536–46. [PubMed: 23669385]
18. Dooley KE, Sayre P, Borland J, Purdy E, Chen S, Song I , et al. Safety, tolerability, and pharmacokinetics of the HIV integrase inhibitor dolutegravir given twice daily with rifampin or once daily with rifabutin: results of a phase 1 study among healthy subjects. J Acquir Immune Defic Syndr. 2013; 62(1): 21–7. [PubMed: 23075918]
19. Song IH, Borland J, Savina PM, Chen S, Patel P, Wajima T , et al. Pharmacokinetics of Single-Dose Dolutegravir in HIV-Seronegative Subjects With Moderate Hepatic Impairment Compared to Healthy Matched Controls. Clin Pharmacol Drug Dev. 2013; 2(4): 342–348. [PubMed: 26097786]
20. Song I, Weller S, Patel J, Borland J, Wynne B, Choukour M , et al. Effect of carbamazepine on dolutegravir pharmacokinetics and dosing recommendation. Eur J Clin Pharmacol. 2016; 72(6): 665–70. [PubMed: 26898568]
21. Song I, Borland J, Chen S, Patel P, Wajima T, Peppercorn A , et al. Effect of food on the pharmacokinetics of the integrase inhibitor dolutegravir. Antimicrob Agents Chemother. 2012; 56(3): 1627–9. [PubMed: 22183173]
22. Weller S, Borland J, Chen S, Johnson M, Savina P, Wynne B , et al. Pharmacokinetics of dolutegravir in HIV-seronegative subjects with severe renal impairment. Eur J Clin Pharmacol. 2014; 70(1): 29–35. [PubMed: 24096683]
23. Ford SL, Gould E, Chen S, Margolis D, Spreen W, Crauwels H , et al. Lack of pharmacokinetic interaction between rilpivirine and integrase inhibitors dolutegravir and GSK1265744. Antimicrob Agents Chemother. 2013; 57(11): 5472–7. [PubMed: 23979733]
24. Johnson M, Borland J, Chen S, Savina P, Wynne B, Piscitelli S. Effects of boceprevir and telaprevir on the pharmacokinetics of dolutegravir. Br J Clin Pharmacol. 2014; 78(5): 1043–9. [PubMed: 24838177]
25. Wang X, Cerrone M, Ferretti F, Castrillo N, Maartens G, Mcclure M , et al. Pharmacokinetics of dolutegravir 100 mg once daily with rifampicin. Int J Antimicrob Agents. 2019; 54(2): 202–206. [PubMed: 31002950]
26. Min S, Song I, Borland J, Chen S, Lou Y, Fujiwara T , et al. Pharmacokinetics and safety of S/GSK1349572, a next-generation HIV integrase inhibitor, in healthy volunteers. Antimicrob Agents Chemother. 2010; 54(1): 254–8. [PubMed: 19884365]
27. Kassahun K, Mcintosh I, Cui D, Hreniuk D, Merschman S, Lasseter K , et al. Metabolism and disposition in humans of raltegravir (MK-0518), an anti-AIDS drug targeting the human immunodeficiency virus 1 integrase enzyme. Drug Metab Dispos. 2007; 35(9): 1657–63. [PubMed: 17591678]
28. Laufer R, Paz OG, Di Marco A, Bonelli F, Monteagudo E, Summa V , et al. Quantitative prediction of human clearance guiding the development of Raltegravir (MK-0518, isentress) and related HIV integrase inhibitors. Drug Metab Dispos. 2009; 37(4): 873–83. [PubMed: 19144773]
29. Mulligan N, Best BM, Wang J, Capparelli EV, Stek A, Barr E , et al. Dolutegravir pharmacokinetics in pregnant and postpartum women living with HIV. AIDS. 2018; 32(6): 729–737. [PubMed: 29369162]
30. Watts DH, Stek A, Best BM, Wang J, Capparelli EV, Cressey TR , et al. Raltegravir pharmacokinetics during pregnancy. J Acquir Immune Defic Syndr. 2014; 67(4): 375–81. [PubMed: 25162818]
31. Waitt C, Orrell C, Walimbwa S, Singh Y, Kintu K, Simmons B , et al. Safety and pharmacokinetics of dolutegravir in pregnant mothers with HIV infection and their neonates: A randomised trial (DolPHIN-1 study). PLoS Med. 2019; 16(9): e1002895. [PubMed: 31539371]
32. Blonk MI, Colbers AP, Hidalgo-Tenorio C, Kabeya K, Weizsacker K, Haberl AE , et al. Raltegravir in HIV-1-Infected Pregnant Women: Pharmacokinetics, Safety, and Efficacy. Clin Infect Dis. 2015; 61(5): 809–16. [PubMed: 25944344]

33. Dallmann A, Ince I, Solodenko J, Meyer M, Willmann S, Eissing T , et al. Physiologically Based Pharmacokinetic Modeling of Renally Cleared Drugs in Pregnant Women. Clin Pharmacokinet. 2017; 56(12): 1525–1541. [PubMed: 28391404]
34. Zhang Z, Unadkat JD. Development of a Novel Maternal-Fetal Physiologically Based Pharmacokinetic Model II: Verification of the model for passive placental permeability drugs. Drug Metab Dispos. 2017; 45(8): 939–946. [PubMed: 28049636]
35. Griessinger JA, Hauptstein S, Laffleur F, Netsomboon K, Bernkop-Schnurch A. Evaluation of the impact of multivalent metal ions on the permeation behavior of Dolutegravir sodium. Drug Dev Ind Pharm. 2016; 42(7): 1118–26. [PubMed: 26552713]
36. Moss DM, Kwan WS, Liptrott NJ, Smith DL, Siccardi M, Khoo SH , et al. Raltegravir is a substrate for SLC22A6: a putative mechanism for the interaction between raltegravir and tenofovir. Antimicrob Agents Chemother. 2011; 55(2): 879–87. [PubMed: 21078936]
37. Open Systems Pharmacology: Compounds: Definition and Work Flows. Acces at: https://docs.open-systems-pharmacology.org/working-with-pk-sim/pk-sim-documentation/pk-sim-compounds-definition-and-work-flow#adme-properties (accessed on February 29, 2020).
38. Poulin P, Schoenlein K, Theil FP. Prediction of adipose tissue: plasma partition coefficients for structurally unrelated drugs. J Pharm Sci. 2001; 90(4): 436–47. [PubMed: 11170034]
39. Poulin P, Theil FP. Prediction of pharmacokinetics prior to in vivo studies. 1. Mechanism-based prediction of volume of distribution. J Pharm Sci. 2002; 91(1): 129–56. [PubMed: 11782904]
40. Rodgers T, Leahy D, Rowland M. Physiologically based pharmacokinetic modeling 1: predicting the tissue distribution of moderate-to-strong bases. J Pharm Sci. 2005; 94(6): 1259–76. [PubMed: 15858854]
41. Rodgers T, Rowland M. Physiologically based pharmacokinetic modelling 2: predicting the tissue distribution of acids, very weak bases, neutrals and zwitterions. J Pharm Sci. 2006; 95(6): 1238–57. [PubMed: 16639716]
42. Takaku T, Nagahori H, Sogame Y, Takagi T. Quantitative structure-activity relationship model for the fetal-maternal blood concentration ratio of chemicals in humans. Biol Pharm Bull. 2015; 38(6): 930–4. [PubMed: 26027836]
43. Nishimura M, Yaguti H, Yoshitsugu H, Naito S, Satoh T. Tissue distribution of mRNA expression of human cytochrome P450 isoforms assessed by high-sensitivity real-time reverse transcription PCR. Yakugaku Zasshi. 2003; 123(5): 369–75. [PubMed: 12772594]
44. Kawade N, Onishi S. The prenatal and postnatal development of UDP-glucuronyltransferase activity towards bilirubin and the effect of premature birth on this activity in the human liver. Biochem J. 1981; 196(1): 257–60. [PubMed: 6796071]
45. Collier AC, Thevenon AD, Goh W, Hiraoka M, Kendal-Wright CE. Placental profiling of UGT1A enzyme expression and activity and interactions with preeclampsia at term. Eur J Drug Metab Pharmacokinet. 2015; 40(4): 471–80. [PubMed: 25465229]
46. Bollen P, Freriksen J, Konopnicki D, Weizsacker K, Hidalgo Tenorio C, Molto J , et al. The Effect of Pregnancy on the Pharmacokinetics of Total and Unbound Dolutegravir and Its Main Metabolite in Women Living With Human Immunodeficiency Virus. Clin Infect Dis. 2020;
47. Jeong H, Choi S, Song JW, Chen H, Fischer JH. Regulation of UDP-glucuronosyltransferase (UGT) 1A1 by progesterone and its impact on labetalol elimination. Xenobiotica. 2008; 38(1): 62–75. [PubMed: 18098064]
48. Dallmann A, Liu XI, Burckart GJ, Van Den Anker J. Drug Transporters Expressed in the Human Placenta and Models for Studying Maternal-Fetal Drug Transfer. The Journal of Clinical Pharmacology. 2019; 59(S70–S81. [PubMed: 31502693]
49. Pfrunder A, Gutmann H, Beglinger C, Drewe J. Gene expression of CYP3A4, ABC-transporters (MDR1 and MRP1-MRP5) and hPXR in three different human colon carcinoma cell lines. J Pharm Pharmacol. 2003; 55(1): 59–66. [PubMed: 12625868]
50. Nakumura T, Sakaeda T, Ohmoto N, Moriya Y, Komoto C, Shirakawa T , et al. Gene expression profiles of ABC transporters and cytochrome P450 3A in Caco-2 and human colorectal cancer cell lines. Pharm Res. 2003; 20(2): 324–7. [PubMed: 12636175]
51. Zrieki A, Farinotti R, Buyse M. Cyclooxygenase inhibitors down regulate P-glycoprotein in human colorectal Caco-2 cell line. Pharm Res. 2008; 25(9): 1991–2001. [PubMed: 18581209]

52. Yano K, Shimizu S, Tomono T, Ogihara T. Gastrointestinal Hormone Cholecystokinin Increases P-Glycoprotein Membrane Localization and Transport Activity in Caco-2 Cells. J Pharm Sci. 2017; 106(9): 2650–2656. [PubMed: 28411043]
53. Sun M, Kingdom J, Baczyk D, Lye SJ, Matthews SG, Gibb W. Expression of the multidrug resistance P-glycoprotein, (ABCB1 glycoprotein) in the human placenta decreases with advancing gestation. Placenta. 2006; 27(6-7): 602–9. [PubMed: 16143395]
54. Wang C, Li H, Luo C, Li Y, Zhang Y, Yun D , et al. The effect of maternal obesity on the expression and functionality of placental P-glycoprotein: Implications in the individualized transplacental digoxin treatment for fetal heart failure. Placenta. 2015; 36(10): 1138–47. [PubMed: 26311557]
55. Bataille A, Rousset J, Marret E, Bonnet F. Ultrasonographic evaluation of gastric content during labour under epidural analgesia: a prospective cohort study. Br J Anaesth. 2014; 112(4): 703–7. [PubMed: 24401801]
56. Davison JS, Davison MC, Hay DM. Gastric emptying time in late pregnancy and labour. J Obstet Gynaecol Br Commonw. 1970; 77(1): 37–41. [PubMed: 5419869]
57. Whitehead EM, Smith M, Dean Y, O'sullivan G. An evaluation of gastric emptying times in pregnancy and the puerperium. Anaesthesia. 1993; 48(1): 53–7. [PubMed: 8434749]
58. Stillhart C, Vucicevic K, Augustijns P, Basit AW, Batchelor H, Flanagan TR , et al. Impact of gastrointestinal physiology on drug absorption in special populations - An UNGAP review. Eur J Pharm Sci. 2020; 105280. [PubMed: 32109493]
59. De Sousa Mendes M, Hirt D, Vinot C, Valade E, Lui G, Pressiat C , et al. Prediction of human fetal pharmacokinetics using ex vivo human placenta perfusion studies and physiologically based models. Brit J Clin Pharmacol. 2016; 81(4): 646–57. [PubMed: 26518984]
60. Schalkwijk S, Buaben AO, Freriksen JJM, Colbers AP, Burger DM, Greupink R , et al. Prediction of Fetal Darunavir Exposure by Integrating Human Ex-Vivo Placental Transfer and Physiologically Based Pharmacokinetic Modeling. Clin Pharmacokinet. 2018; 57(6): 705–716. [PubMed: 28744795]
61. Liu XI, Momper JD, Rakhmanina N, Van Den Anker JN, Green DJ, Burckart GJ , et al. Physiologically Based Pharmacokinetic Models to Predict Maternal Pharmacokinetics and Fetal Exposure to Emtricitabine and Acyclovir. The Journal of Clinical Pharmacology. 2019;
62. Schalkwijk S, Greupink R, Colbers AP, Wouterse AC, Verweij VG, Van Drongelen J , et al. Placental transfer of the HIV integrase inhibitor dolutegravir in an ex vivo human cotyledon perfusion model. J Antimicrob Chemother. 2016; 71(2): 480–3. [PubMed: 26538508]
63. Hill MD, Abramson FP. The significance of plasma protein binding on the fetal/maternal distribution of drugs at steady-state. Clinical pharmacokinetics. 1988; 14(3): 156–170. [PubMed: 3286084]
64. Chignell CF, Vesell ES, Starkweather DK, Berlin CM. The binding of sulfaphenazole to fetal, neonatal, and adult human plasma albumin. Clin Pharmacol Ther. 1971; 12(6): 897–901. [PubMed: 5134994]
65. Krasner J, Giacoia GP, Yaffe SJ. Drug-protein binding in the newborn infant. Ann N Y Acad Sci. 1973; 226(101–14. [PubMed: 4520389]
66. Herve F, Rajkowski K, Martin MT, Dessen P, Cittanova N. Drug-binding properties of rat alpha 1-foetoprotein. Binding of warfarin, phenylbutazone, azapropazone, diazepam, digitoxin and cholic acid. Biochem J. 1984; 221(2): 401–6. [PubMed: 6206846]
67. Hirano K, Watanabe Y, Adachi T, Ito Y, Sugiura M. Drug-binding properties of human alpha-foetoprotein. Biochem J. 1985; 231(1): 189–91. [PubMed: 2415113]
68. U.S. Food and Drug Administration: FDA Drug Safety Communication: FDA to evaluate potenitial risk of neural tube birth defects with HIV medicine dolutegravir (Juluca, Tivicay, Triumeq). . Https://www.fda.gov/Drugs/DrugSafety/ucm608112.htm (accessed on June 25, 2018).
69. WHO: Potential safety issue affecting women living with HIV using dolutegravir at the time of conception. Access at: http://www.who.int/medicines/publications/drugalerts/Statement_on_DTG_18May_2018final.pdf (accessed on November 11, 2019). 2018;

70. Zamek-Gliszczynski MJ, Zhang X, Mudunuru J, Du Y, Chen JL, Taskar KS , et al. Clinical Extrapolation of the Effects of Dolutegravir and Other HIV Integrase Inhibitors on Folate Transport Pathways. Drug Metab Dispos. 2019; 47(8): 890–898. [PubMed: 31167838]
71. Moss DM, Siccardi M, Murphy M, Piperakis MM, Khoo SH, Back DJ , et al. Divalent metals and pH alter raltegravir disposition in vitro. Antimicrob Agents Chemother. 2012; 56(6): 3020–6. [PubMed: 22450971]
72. Moss DM, Siccardi M, Back DJ, Owen A. Predicting intestinal absorption of raltegravir using a population-based ADME simulation. J Antimicrob Chemother. 2013; 68(7): 1627–34. [PubMed: 23515248]
73. Iwamoto M, Wenning LA, Petry AS, Laethem M, De Smet M, Kost JT , et al. Minimal effects of ritonavir and efavirenz on the pharmacokinetics of raltegravir. Antimicrob Agents Chemother. 2008; 52(12): 4338–43. [PubMed: 18838589]
74. Iwamoto M, Wenning LA, Petry AS, Laethem M, De Smet M, Kost JT , et al. Safety, tolerability, and pharmacokinetics of raltegravir after single and multiple doses in healthy subjects. Clin Pharmacol Ther. 2008; 83(2): 293–9. [PubMed: 17713476]
75. Markowitz M, Morales-Ramirez JO, Nguyen BY, Kovacs CM, Steigbigel RT, Cooper DA , et al. Antiretroviral activity, pharmacokinetics, and tolerability of MK-0518, a novel inhibitor of HIV-1 integrase, dosed as monotherapy for 10 days in treatment-naive HIV-1-infected individuals. J Acquir Immune Defic Syndr. 2006; 43(5): 509–15. [PubMed: 17133211]
76. Rhee EG, Rizk ML, Brainard DM, Gendrano IN 3rd, Jin B, Wenning LA , et al. A pharmacokinetic comparison of adult and paediatric formulations of raltegravir in healthy adults. Antivir Ther. 2014; 19(6): 619–24. [PubMed: 24608069]
77. Wenning LA, Hanley WD, Brainard DM, Petry AS, Ghosh K, Jin B , et al. Effect of rifampin, a potent inducer of drug-metabolizing enzymes, on the pharmacokinetics of raltegravir. Antimicrob Agents Chemother. 2009; 53(7): 2852–6. [PubMed: 19433563]
78. Iwamoto M, Wenning LA, Nguyen BY, Teppler H, Moreau AR, Rhodes RR , et al. Effects of omeprazole on plasma levels of raltegravir. Clin Infect Dis. 2009; 48(4): 489–92. [PubMed: 19143531]
79. Brainard DM, Friedman EJ, Jin B, Breidinger SA, Tillan MD, Wenning LA , et al. Effect of low-, moderate-, and high-fat meals on raltegravir pharmacokinetics. J Clin Pharmacol. 2011; 51(3): 422–7. [PubMed: 20457591]
80. Taburet AM, Sauvageon H, Grinsztejn B, Assuied A, Veloso V, Pilotto JH , et al. Pharmacokinetics of Raltegravir in HIV-Infected Patients on Rifampicin-Based Antitubercular Therapy. Clin Infect Dis. 2015; 61(8): 1328–35. [PubMed: 26105170]

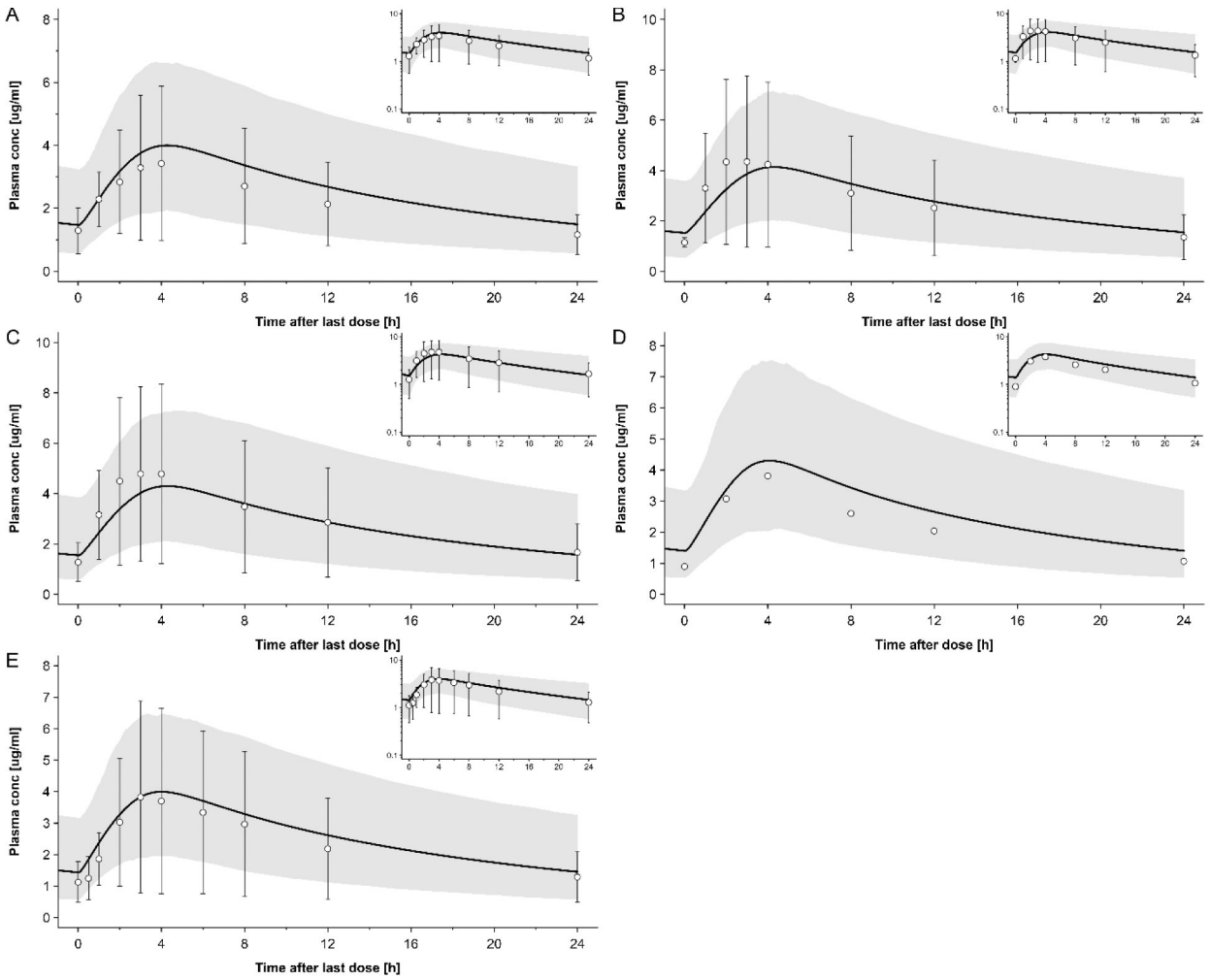

Figure 1:

Plasma concentration-time profiles of dolutegravir following oral administration once a day of 50 mg in fed state in non-pregnant subjects. Circles represent observed *in vivo* data from following studies: **A**: Ford et al [23]; **B**: group 1 of the study from Johnson et al [24]; **C**: group 2 of the study from Johnson et al [24]. **D**: Wang et al [25]; E: Song et al [20]; The solid line represents the simulated plasma concentration in different population and the shaded area is the predicted 5^{th} – 95^{th} percentile range. Semi-log scale figures are given as inset figure in the top right corners.

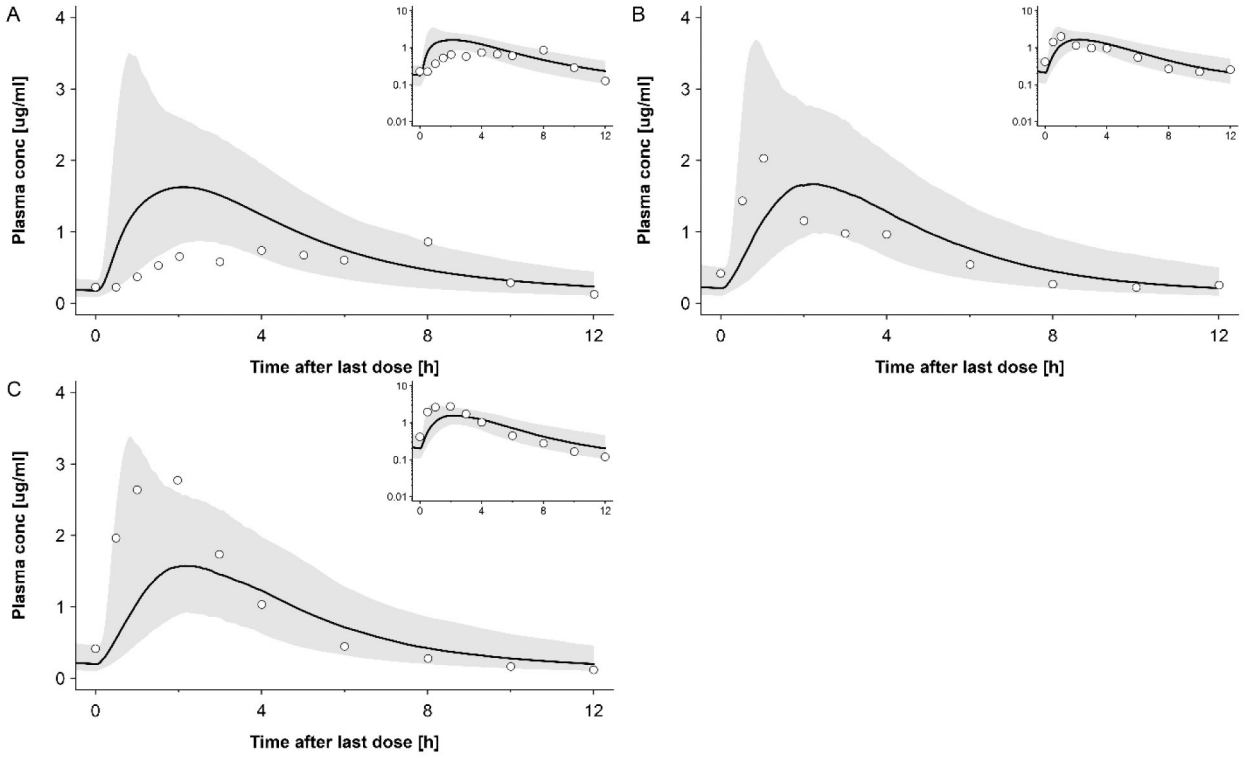

Figure 2:

Plasma concentration-time profiles of raltegravir following oral administration twice a day of 400mg with moderate fat meal in non-pregnant subjects. Circles represent observed *in vivo* data from following studies: **A**: Brainard et al [79]; **B**: group 1 of the study from Taburet et al [80]; **C**: group 2 of the study from Taburet et al[80]. The solid line represents the simulated plasma concentration in different population and the shaded area is the predicted 5^{th} – 95^{th} percentile range. Semi-log scale figures are given as inset figure in the top right corners.

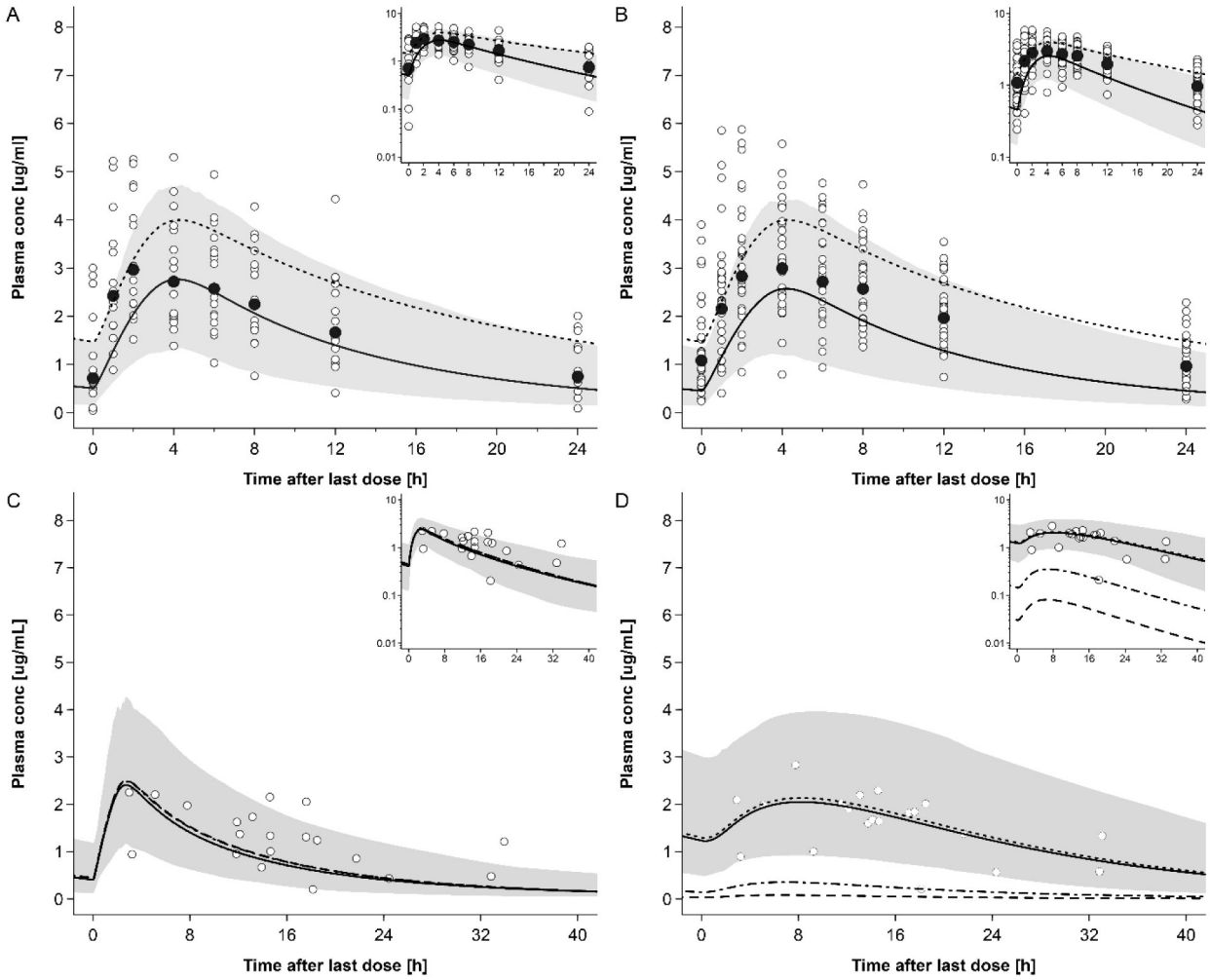

Figure 3:

Plasma concentration-time profiles of dolutegravir following oral administration of 50 mg once a day in pregnant women. Semi-log scale figures are given as inset figure in the top right corners. Observed steady-state *in vivo* data were taken from *in vivo* study of IMPAACT P1026. [29] **A**: dolutegravir 50 mg once a day in pregnant women in 2nd trimester. Empty circles represent individual concentrations taken from *in vivo* study of IMPAACT P1026. [29] Black circles represent geometric mean concentrations taken from *in vivo* study of IMPAACT P1026. [29] The solid line represents the predicted mean concentration and the shaded area the predicted 5th – 95th percentile range; The dotted line represents the predicted mean concentration of non-pregnant population; **B**: dolutegravir 50 mg once a day in pregnant women in 3rd trimester. Empty circles represent individual concentrations taken from *in vivo* study of IMPAACT P1026. [29] The solid line represents the predicted mean concentration and the shaded area the predicted 5th – 95th percentile range; The dotted line represents the predicted mean concentration of non-pregnant population; **C**: dolutegravir 50 mg once a day in pregnant women with an average gestational age of 38 weeks at delivery. Empty circles represent individual concentration data in the maternal plasma taken from *in vivo* study of IMPAACT P1026. [29]; the lines

represent the predicted mean concentration in the maternal plasma using different partition coefficients calculated by different methods.; The solid line represents the QSAR method; The dotted line represents Poulin and Theil method; The dash-dot line represents the Rodgers and Rowland method; The dash line represents the PK-sim standard method. The shaded area represents the predicted 5^{th} – 95^{th} percentile range of the prediction by using QSAR method. **D**: dolutegravir 50 mg once a day in pregnant women with an average gestational age of 38 weeks at delivery. Empty circles represent individual concentration data in the umbilical vein taken from *in vivo* study of IMPAACT P1026; [29] the lines represent the predicted mean concentration in the umbilical vein using different partition coefficients calculated by different methods: the solid line represents the QSR method; the dotted line represents Poulin and Theil method; the dash-dot line represents the Rodgers and Rowland method; and the dash line represents the PK-sim standard method. The shaded area presents the predicted 5^{th} – 95^{th} percentile range of the prediction by using QSAR method.

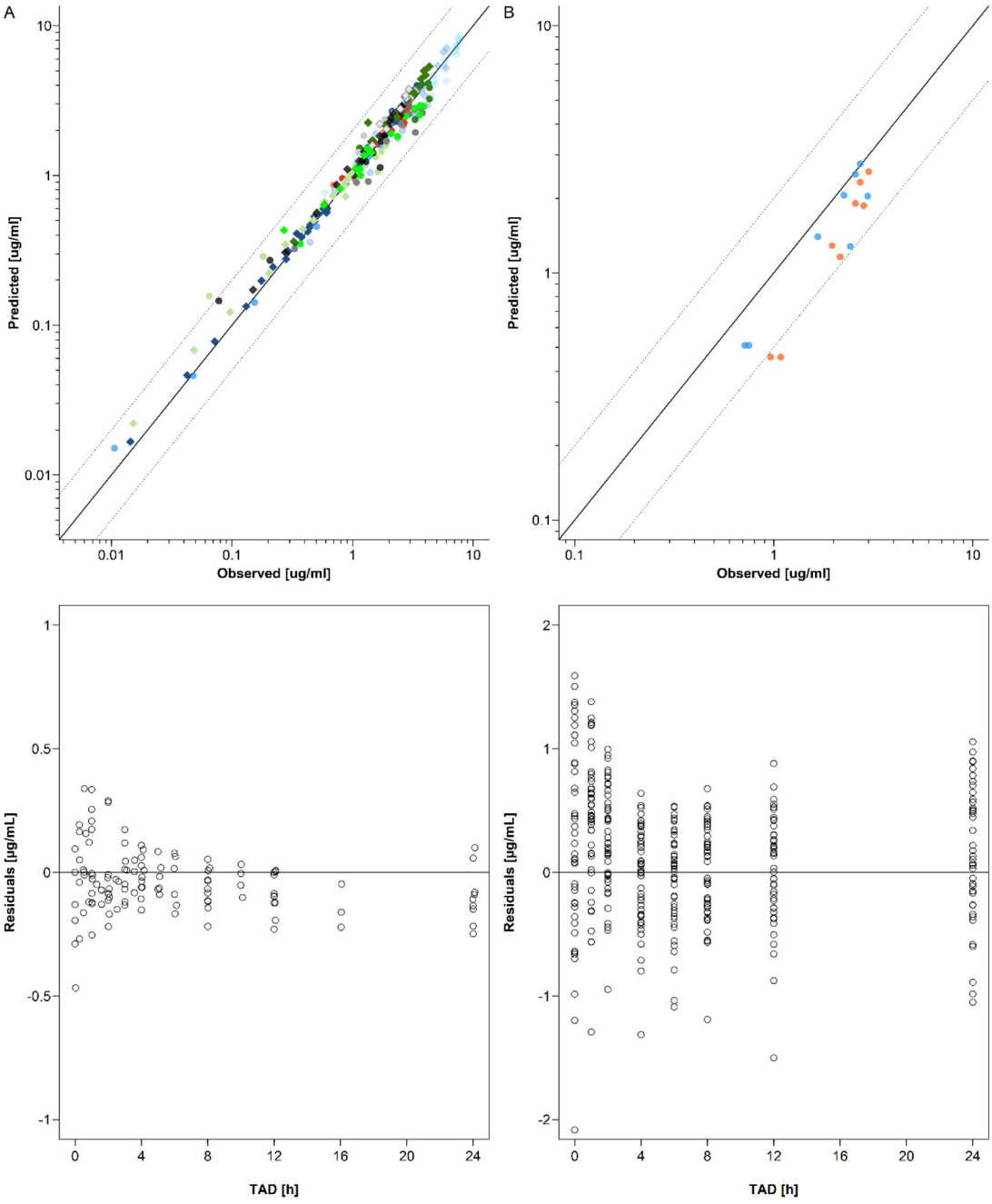

Figure 4:

Goodness-of-fit and residuals vs time plots of dolutegravir concentrations in non-pregnant subjects (A) and pregnant women (B). The solid line represents the line of identity and the dotted lines the 2-fold error range. **A panel**: Upper plot: GOF plot of geometric mean dolutegravir concentrations in non-pregnant populations. single dose study: blue circles indicate the study by Castellino et al. (20mg single dose) [17]; green circles indicate the study by Song et al. (50mg single dose) [19]; light blue circles indicate the high fat meal group in the study by Song et al. (50mg single dose) [21]; black circles indicate the study by Weller et al. (50mg single dose) [22]; bright green circles indicate the moderate fat meal

group in the study by Song et al. (50mg single dose) [21]; grey circles indicate the low fat meal group in the study by Song et al. (50mg single dose) [21]. multiple dose study: dark blue circles indicate the study by Ford et al. (50mg once daily) [23]; orange circles indicate the group 1 in the study by Dooley et al. (50mg once daily)[18]; red circles indicate the group 2 in the study by Dooley et al. (50mg once daily)[18]; dark green circles indicate the group 1 in the study by Johnson et al. (50mg once daily) [24]; sky blue circles indicate the group 2 in the study by Johnson et al. (50mg once daily) [24]; light grey circles indicate the study by Song et al. (50mg once daily) [20]; yellow circles indicate the study by Wang et al. (50mg once daily)[25]. Lower plot: residuals vs time plot of dolutegravir in non-pregnant population. empty circles represent the geometric mean concentrations of non-pregnancy reference studies. **B panel**: Upper plot: GOF plot of dolutegravir in pregnant population. Blue circles indicate geometric mean concentrations in 2^{nd} trimester and orange circles indicate geometric mean concentrations in 3^{rd} trimester; Lower plot: residuals vs time plot of dolutegravir in pregnant population. Empty circles represent the individual concentrations in 2^{nd} and 3^{rd} trimesters.

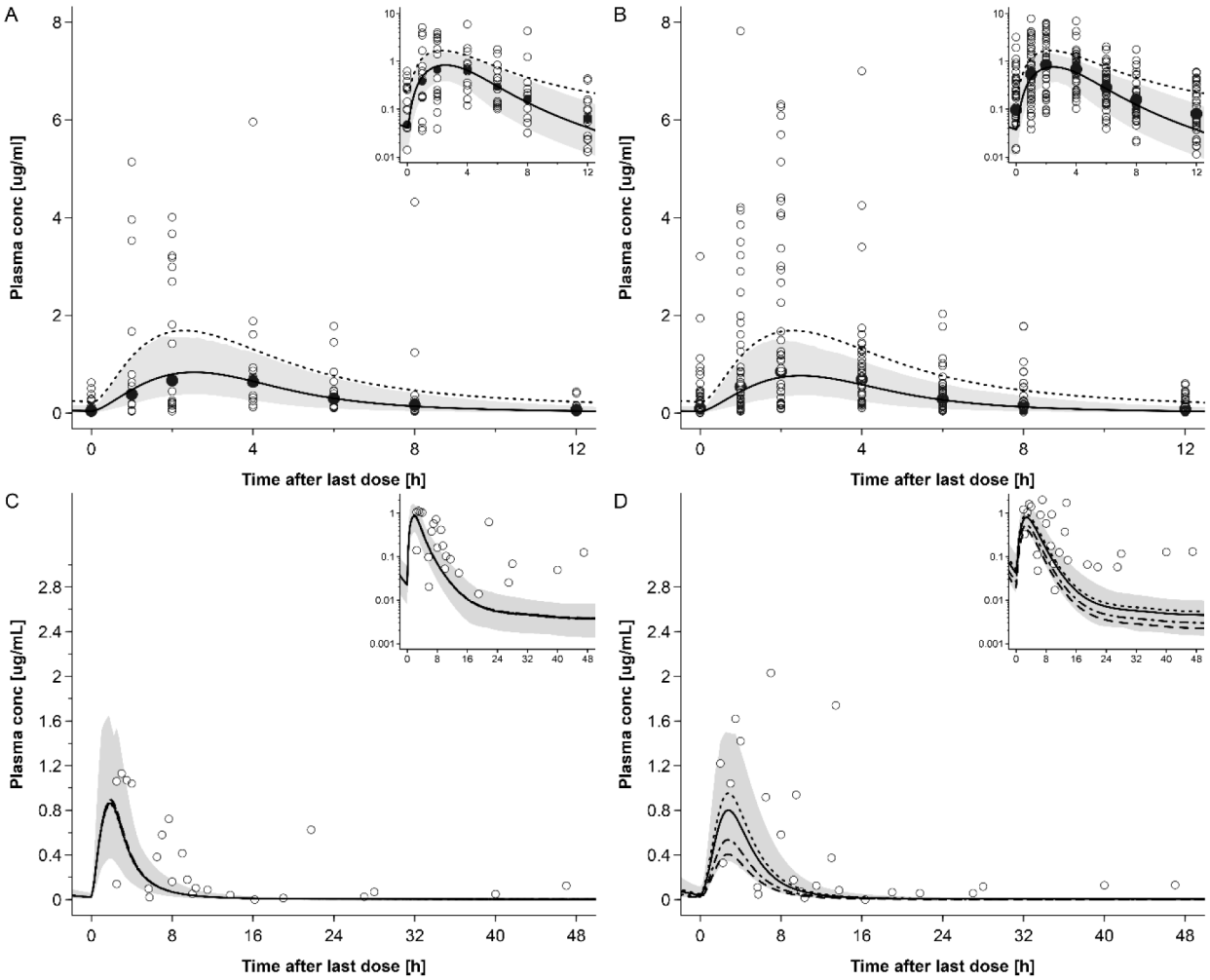

Figure 5:

Plasma concentration-time profiles of raltegravir following oral administration of 400 mg twice a day in pregnant women in steady state. Semi-log scale figures are given as inset figure in the top right corners. Observed steady-state *in vivo* data were taken from *in vivo* study of IMPAACT P1026.[30] **A**: raltegravir 400 mg twice a day in pregnant women in 2nd trimester. Empty circles represent individual concentrations taken from *in vivo* study of IMPAACT P1026. [30] Black circles represent geometric mean concentrations taken from *in vivo* study of IMPAACT P1026. [30] The solid line represents the predicted mean concentration and the shaded area the predicted 5th – 95th percentile range; The dotted line represents the predicted mean concentration of non-pregnant population; **B**: raltegravir 400 mg twice a day in pregnant women in 3rd trimester. Empty circles represent individual concentrations taken from *in vivo* study of IMPAACT P1026. [30] The solid line represents the predicted mean concentration and the shaded area the predicted 5th – 95th percentile range; The dotted line represents the predicted mean concentration of non-pregnant population; **C**: raltegravir 400 mg twice a day in pregnant women with an average gestational age of 38 weeks at delivery. Empty circles represent individual concentration data in the maternal plasma taken from *in vivo* study of IMPAACT P1026; [30] the lines

represent the predicted mean concentrations in the maternal plasma using different partition coefficients calculated by different methods.; The solid line represents the QSAR method; The dotted line represents Poulin and Theil method; The dash-dot line represents the Rodgers and Rowland method; The dash line represents the PK-sim standard method. The shaded area represents the predicted 5^{th} – 95^{th} percentile range of the prediction by using QSAR method. **D**: raltegravir 400 mg twice a day in pregnant women with an average gestational age of 38 weeks at delivery. Empty circles represent individual concentration data in the umbilical vein taken from *in vivo* study of IMPAACT P1026; [30] the lines represent the predicted mean concentrations in the umbilical vein using different partition coefficients calculated by different methods: the solid line represents the QSAR method; the dotted line represents Poulin and Theil method; the dash-dot line represents the Rodgers and Rowland method; and the dash line represents the PK-sim standard method. The shaded area represents the predicted 5^{th} – 95^{th} percentile range of the prediction by using QSAR method.

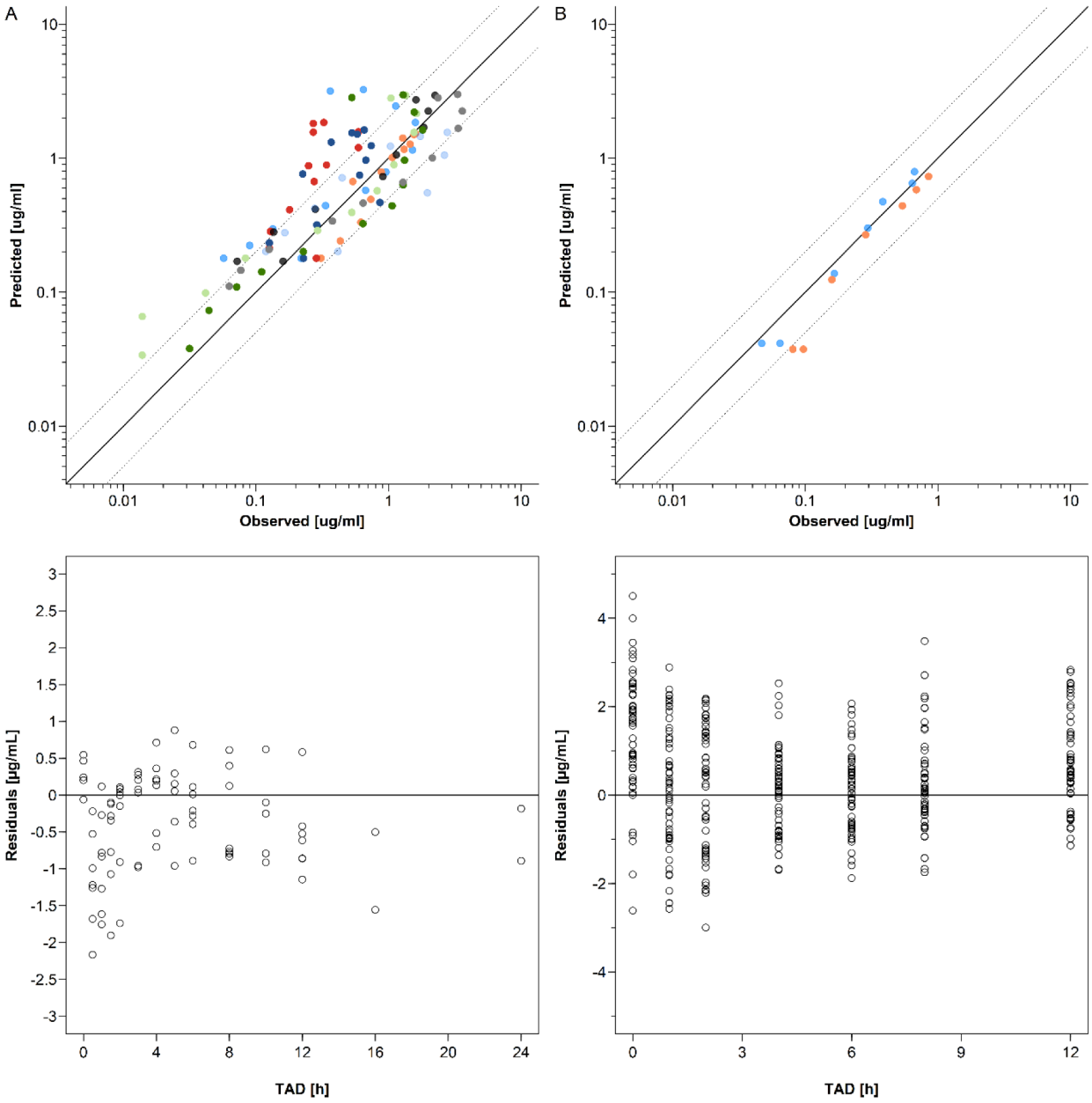

Figure 6:

Goodness-of-fit and residuals vs time plots of raltegravir concentrations in non-pregnant subjects (A) and pregnant women (B). The solid line represents the line of identity and the dotted lines the 2-fold error range. **A panel**: Upper plot: GOF plot of geometric mean dolutegravir concentrations in non-pregnant populations. single dose study: bright green circles indicate the study by Iwamoto et al. (400mg single dose) [78]; dark green circles indicate the study by Rhee et al. (400mg single dose) [76]; grey circles indicate the study by Wenning et al. (400mg single dose) [77]. multiple dose study: blue circles indicate the fasted group in the study by Brainard et al. (400mg multiple dose) [79]; orange circles indicate the high fat group in the study by Brainard et al. (400mg multiple dose)[79]; dark blue circles indicate high moderate fat group in the study by Brainard et al. (400mg multiple dose) [79];

red circles indicate the low fat group in the study by Brainard et al. (400mg multiple dose) [79]; black circles indicate the study by Markowitz et al. (400mg multiple dose) [75]. sky blue circles indicate the group 1 in the study by Taburet et al. (400mg multiple dose) [80]; light blue circles indicate the group 2 in the study by Taburet et al. (400mg multiple dose) [80]; **B panel**: Upper plot: GOF plot of raltegravir in pregnant population. blue circles indicate geometric mean concentrations in women in the 2nd trimester; orange circles indicate geometric mean concentrations in women in the 3rd trimester. Lower plot: residuals vs time plot of raltegravir in pregnant population. Empty circles represent the individual concentrations in 2nd and 3rd trimesters.

Table 1:

Summary of input data for PBPK models in non-pregnant subjects

	Dolutegravir		Raltegravir	
Parameter [unit]	**Value**	**Reference**	**Value**	**Reference**
Molecular weight [g/mol]	419.38	Drugbank.ca	444.42	Drugbank.ca
Lipophilicity [log units]	0.98	*fitted* [a]	0.58	Moss et al. [71]
pK_a (acid)	10.1	Drugbank.ca	6.67	Moss et al. [71]
Fraction unbound:				
Non-pregnant	7.0E-3	Clinical Pharmacology and Biopharmaceutics Review[16]	0.170	Laufer et al. [28]
2nd trimester	8.4E-3	*calculated*	0.198	*calculated*
3rd trimester	8.8E-3	*calculated*	0.206	*calculated*
Major binding protein	Albumin	Drugbank.ca	Albumin	Laufer et al. [28]
Solubility (at pH 7) [mg/L]	0.172[c]; 1.98[d]; 0.0252[e]	*fitted* [a]	8900 [f]	Moss et al. [72]
Intestinal permeability (transcellular) [cm/min]	0.05	*fitted* [a]	$1.71 \cdot 10^{-5}$	*fitted* [g]
Model for estimating organ-to-plasma partition coefficients	Rogers & Rowland		Rogers & Rowland	
GFR fraction			1.0	Kassahun et al. [27]
$K_{m\text{-}UGT1A1}$ [uM]	149	Reese et al. [12]	99	Kassahun et al. [27]
$V_{max\text{-}UGT1A1}$ [nmol/min/mg]	7.34	*fitted* [a]	2.74 [d]	*fitted* [g]
$K_{m\text{-}UGT1A9}$ [uM]			296	Kassahun et al. [27]
$V_{max\text{-}UGT1A9}$ [nmol/min/mg] CLspec/[Enzyme$_{_CYP3A4}$] [1/umol/min]	0.05	*fitted* [a]	1.63 [d]	*fitted* [g]

[a]Value simultaneously fitted to *in vivo* plasma concentration-time profiles of non-pregnant subjects and to the reported dose fractions metabolized [17-26].

[b]Solubility for the suspension

[c]Solubility for the tablet formulation administered in fasted state

[d]Solubility for the tablet formulation administered in fed state

[e]Solubility for the suspension

[f]Solubility implemented as table: PH=1 to 4, solubility=40mg/L; PH=5, solubility=120mg/L; PH=6, solubility=980mg/L; PH=7, solubility=8900mg/L; PH=8, solubility=37300mg/L.

[g]Value fitted to *in vivo* pharmacokinetic data of non-pregnant subjects following oral administration [27, 73-77].

Abbreviations: GFR: glomerular filtration rate; PBPK: physiologically based pharmacokinetic

Table 2:

Values for the partition coefficient between the fetal intracellular space and the maternal blood plasma ($K_{fc:mp}$) calculated according to different method

Drug	Method PK-Sim Standard	Poulin & Theil	Rodgers & Rowland	QSAR
Dolutegravir	0.0085	0.43	0.04	0.40
Raltegravir	0.19	0.52	0.26	0.42

Table 3:

Enzymes amount included in fetal compartments of the PBPK model

Tissue	Enzyme amount [µmol]		
	CYP3A4	UGT1A1	UGT1A9
Fetal part of the placenta	3.98E-4	0.06	NA
Fetus	0.12	0.03	0.024

Table 4:

Comparison of simulated or predicted and observed PK Parameters

	$AUC_{0\text{-}t/\infty}$ [mg ·h/L][a] Simulated/ observed (ratio)	C_{max} [mg/L] Simulated/ observed (ratio)	t_{max} [h] Simulated/ observed (ratio)
Dolutegravir			
Non-pregnant women			
Castellino study [17]	34.0/35.9 (0.95)	2.29/2.53 (0.86)	0.95/0.50 (1.90)
Dooley study cohort 1 [18] (steady state)	39.0/36.1 (1.08)	2.91/2.65 (1.10)	2.25/1.5 (1.50)
Dooley study cohort 2 [18] (steady state)	41.1/42.1 (0.98)	2.96/2.91 (1.02)	2.20/2.00 (1.10)
Ford study [23] (steady state)	63.1/52.5(1. 20)	4.00/3.43 (1.17)	4.25/4.00 (1.06)
Johnson2014, Cohort 1 (steady state) [24]	65.2/71.9 (0.91)	4.14/4.35 (0.95)	4.30/3.00 (1.43)
Johnson2014, Cohort2 (steady state) [24]	67.4/71.9 (0.94)	4.30/4.78 (0.90)	4.30/3.50 (1.23)
Song2012_high_fat [21]	66.1/83.6 (0.79)	2.97/4.19 (0.71)	4.90/5.00 (0.98)
Song2012_low_fat [21]	59.8/66.7 (0.90)	2.83/3.81 (0.74)	4.00/3.00 (1.33)
Song2012_moderate_fat [21]	64.7/71.0 (0.91)	2.94/3.86 (0.76)	4.75/4.00 (1.19)
Song2016_moderate_fat_meal [20] (steady state)	62.2/55.4 (1.12)	3.99/3.83 (1.04)	4.00/3.00 (1.33)
Song2013 study [19] [b]	47.2/40.3 (1.17)	1.82/1.90 (0.96)	2.50/3.00 (0.83)
Weller study [22]	44.1/37.1 (1.19)	1.89/1.84 (1.03)	2.40/2.50 (0.96)
Wang2019 [25]	63.8/51.62 (1.23)	4.30/3.81(1.13)	4.10/4.00 (1.03)
Pregnant women			
2nd trimester (steady state)	34.70/42.38 (0.82)	2.77/3.00 (0.92)	4.20/2.00 (2.10)
3rd trimester (steady state)	31.91/47.59 (0.67)	2.57/3.00 (0.86)	4.20/4.00 (1.05)
Raltegravir			
Non-pregnant women	See OSP GitHub	See OSP GitHub	See OSP GitHub
Markowitz2006[75]	8.86/7.96 (1.11)	3.04/2.24 (1.36)	0.80/1.00 (0.80)
Iwamoto2009[78]	8.66/4.90 (1.77)	3.10/1.28 (2.42)	0.75/1.50 (0.50)
Rhee2014 [76]	9.13/8.53 (1.07)	3.11/2.22 (1.40)	0.75/2.00 (0.38)
Wenning2009 [77]	8.99/12.25 (0.73)	3.12/3.82 (0.81)	0.75/1.50 (0.50)
Brainard2011_fasted [b] [79]	9.66/6.47 (1.49)	3.42/1.59 (2.15)	0.75/2.00 (0.38)
Brainard2011_high fat [b] [79]	8.83/ 11.37 (0.78)	1.48/1.59 (0.93)	2.45/2.00 (1.23)
Brainard2011_moderate_fat [b] [79]	8.86/6.44 (1.38)	1.54/0.74 (2.08)	2.20/4.00 (0.55)
Brainard2011_low_fat [b] [79]	9.01/3.39 (2.66)	1.76/0.59 (2.98)	1.95/3.50 (0.56)
Taburet2015_moderate_fat_1 [c] [80]	8.46/8.24 (1.03)	1.65/2.03 (0.82)	2.20/1.00 (2.20)
Taburet2015_moderate_fat_2 [c] [80]	8.95/ 11.00 (0.81)	1.54/2.77 (0.56)	2.20/2.00 (1.10)
Pregnant women			
2nd trimester (steady state)	4.10/3.90 (1.05)	0.834/0.67 (1.22)	2.55/2.00 (1.28)
3rd trimester (steady state)	3.71/4.44 (0.84)	0.763/0.85 (0.89)	2.50/2.00 (1.25)

Data expressed as geometric mean values unless indicated otherwise.

[a] AUC_{0-t} was used in the studies by Dooley et al. [18], Ford et al. [23], Johnson et al. [24], Song et al. [20], Markowitz et al.,[75] Brainard et al. [79] and Taburet et al.[80]; whereas $AUC_{0-\infty}$ was used in the studies by Castellino et al. [17], Song et al. [21], Song et al. [19], Weller et al. [22], Iwamoto et al.[78], Rhee et al.[76] and Wenning et al.[77].

[b] Data expressed as arithmetic mean values.

[c] Data expressed as median values.

Abbreviations: AUC_{0-t}: area under the concentration-time curve from zero to the time point of the last observed plasma concentration (in case of multiple dose studies, time refers to the time after last dose); $AUC_{0-\infty}$: area under the concentration-time curve from zero to infinity; C_{max}: peak plasma concentration; t_{max}: time at which peak plasma concentration is reached.